

CrossMark
click for updatesCite this: *CrystEngComm*, 2016, 18, 9334

The role of PLLA-*g*-montmorillonite nanohybrids in the acceleration of the crystallization rate of a commercial PLA†

Nerea Zaldua,^a Agurtzane Mugica,^a Manuela Zubitur,^{ab} Amaia Iturrospe,^c Arantxa Arbe,^c Giada Lo Re,^{de} Jean-Marie Raquez,^d Philippe Dubois^{df} and Alejandro J. Müller^{*ag}

Employing the hydroxyl groups on the surface of Cloisite® 30B montmorillonite (Cl30B), the ring-opening polymerization of L-lactide was performed with a metal-free catalyst to yield a PLLA-*g*-Cl30B nanohybrid with low M_n grafted PLLA chains (*i.e.*, 9 kg mol⁻¹). This nanohybrid was then melt mixed with PLA 4032D from NatureWorks, which is a slow-crystallizing PLA as it contains 2% D-isomers and has a high M_n value (*i.e.*, 123 kg mol⁻¹). The samples were characterized by TEM, WAXS, SAXS, DSC and Polarized Light Optical Microscopy (PLOM) in order to study their crystallization kinetics in depth. The dispersion of the nanoclay was excellent and much better in the PLA/PLLA-*g*-Cl30B nanocomposites in comparison to PLA/Cl30B blends prepared as reference. In order to ascertain the role of the nanoclay, analogue PLA/PLLA blends without Cl30B were also prepared. The spherulitic crystallization kinetics from the melt was determined for all samples. The growth rate of neat PLA was accelerated approximately 3 times by incorporating the PLLA-*g*-Cl30B nanohybrid with an inorganic content of 5%. The overall crystallization kinetics from the glassy state of PLA was also accelerated in a similar way by the nanohybrid addition. Nevertheless, the PLA/PLLA blends crystallized even faster indicating that the dominant effect that causes the acceleration of the crystallization of PLA is the plasticization of PLA by the low M_n PLLA molecules. The changes in T_g of PLA also support this explanation. In the case of the PLA/PLLA-*g*-Cl30B nanocomposites, even though the plasticizing effect of the PLLA chains still dominates, their action is counterbalanced by their tethering on one end, as they are grafted to the surface of the exfoliated clay nanoplatelets.

Received 16th September 2016,
Accepted 31st October 2016

DOI: 10.1039/c6ce02005d

www.rsc.org/crystengcomm

Introduction

Biodegradable polymers produced from renewable resources are attracting much attention in view of the growing concerns for the environment.¹

In this respect, polylactide (PLA) is a commercially available bio-based aliphatic polyester that is biodegradable, melt-processable and has acceptable mechanical properties for certain applications where toughness is not required.^{2,3}

Broader applications of PLA are limited by its slow crystallization rate, brittle behaviour and sensitivity to hydrolysis. In order to widen its applications to fields like automotives and electronics, the performance of this polymer has to be substantially improved.^{4,5}

The addition of nanofillers, such as layered aluminosilicate clays, is one possible method to improve some of the properties of PLA, because even with a very low nanofiller content, these nanocomposites exhibit better properties as compared with pristine polymers, including improved mechanical properties, thermal resistance, gas barrier properties, and fire retardancy.^{6–9}

In order to obtain the best improvement in the properties of PLA/nanofiller nanocomposites, exfoliated nanocomposites should be produced. A successful way to achieve this goal is the “grafting from” approach, where polymer chains are grafted on the nanoclay by polymerization from its surface.¹⁰

^a POLYMAT and Polymer Science and Technology Department, Faculty of Chemistry, University of the Basque Country UPV/EHU, Paseo Manuel de Lardizabal 3, 20018 Donostia-San Sebastián, Spain. E-mail: alejandrojesus.muller@ehu.es

^b Chemical and Environmental Engineering Department, Polytechnic School, University of the Basque Country UPV/EHU, 20018 Donostia-San Sebastián, Spain

^c Centro de Física de Materiales (CFM) (CSIC-UPV/EHU) - Materials Physics Center (MPC), Paseo Manuel de Lardizabal 5, 20018 San Sebastián, Spain

^d Service des Matériaux Polymères et Composites, Centre d'Innovation et de Recherche en Matériaux Polymères CIRMAP, Université de Mons, Place du Parc 23, B-7000 Mons, Belgium

^e Fibre and Polymer Technology/WWSC - Division of Biocomposites, School of Chemical Science and Engineering, KTH Royal Institute of Technology, Teknikringen 56, SE-100 44 Stockholm, Sweden

^f MRT Dpt, Luxembourg Institute of Science and Technology - LIST, Luxembourg

^g IKERBASQUE, Basque Foundation for Science, Bilbao, Spain

† Electronic supplementary information (ESI) available. See DOI: 10.1039/c6ce02005d

Several researchers have prepared polyester-functionalized montmorillonite clays (MMT-clays) by the “grafting from” method.^{1,11,12} The results evidenced improved interactions between nanofillers and the matrix that lead to the production of nanocomposites with a high degree of exfoliation.

Even if this chemical “grafting from” approach is an efficient method for obtaining exfoliated clay nanocomposites, melt blending is the most established technique to process thermoplastic polymers from an industrial point of view.

Employing a polymer/clay masterbatch can combine the high degree of exfoliation obtained in polymer-grafted clay and the practicality of melt blending. In this method, a polymer-grafted clay with a high clay content is obtained *via* “grafting from” and is redispersed by melt-mixing in a PLA matrix. This process has been performed before with poly(ϵ -caprolactone).^{13,14}

In the case of PLA, Paul *et al.* prepared poly(L-lactide) (PLLA) layered silicate (nano)composites by intercalative *in situ* polymerization of L-lactide in the presence of a montmorillonite organo-modified with ammonium cations bearing primary hydroxyl groups (*i.e.*, Cloisite® 30B).¹⁵ The obtained “grafted” nanocomposite was used as a masterbatch for melt-mixing with a commercial PLA matrix at an inorganic loading of 3 wt%. They found that the exfoliation level obtained with the masterbatch was higher than that obtained directly by melt blending with Cloisite 30B. They did not observe any change in the T_g of the matrix and, whereas in conventional melt blending, the PLLA matrix remained amorphous, in the case of the masterbatch nanocomposite, a relatively low enthalpy of melting was detected for the PLA component. The authors suggested that this result is a consequence of the nucleating action of short-chain PLLA grafted onto Cloisite® 30B.

Urbanczyk *et al.* used supercritical carbon dioxide as a polymerization medium for the *in situ* polymerization of D,L-lactide in the presence of organo-modified MMT-clays.¹⁶ The nanocomposites obtained using Cloisite® 30B, containing PLA grafted chains, were melt mixed with commercial PLA to reach a final clay content of 3 wt%. X-ray scattering and TEM analysis showed that a good exfoliation degree had been achieved. They obtained an increase in the PLA modulus (up to 20%) and a slight increase in impact resistance.

Other authors have used different nanofillers grafted to PLLA.^{17–19}

More recently, Lo Re *et al.* prepared polyester-functionalized MMT-clay nanohybrids *via* ring-opening polymerization (ROP) of L- and D-lactide with hydroxyl-functionalized Cloisite® 30B.²⁰ They used a metal-free catalyst (1,8-diazabicyclo[5.4.0]undec-7-ene) instead of common metal-based catalysts like tin(II) octoate. The PL(D)LA-based nanohybrids were redispersed into high molecular weight PLA using melt blending techniques. Their goal was to investigate the effect of the addition of layered silicate nanofillers and stereocomplexation on its thermal, mechanical and barrier properties.

Lo Re *et al.* found that in the case of PL(D)LA nanocomposites based on grafted clay, almost complete exfolia-

tion was achieved as compared with the nanocomposite based on pristine Cloisite® 30B. The storage modulus measured by DMTA showed an increase for nanocomposites based on grafted clay at temperatures below the glass transition temperature, a result connected with the improved dispersion of nanoclay obtained by the “grafting from” method. The grafted clay nanocomposites exhibited a decrease in the relative oxygen permeability of 41% in comparison with a decrease of 32% for nanocomposites based on pristine Cloisite® 30B. The enhancement in the properties was higher when stereocomplexation had been achieved.

The effectiveness of melt blending a PLA-grafted clay with a PLA matrix in order to improve the clay dispersion and, therefore, to obtain improved properties has been previously studied in the literature; however, to our knowledge, an in-depth study of the crystallization behavior of such materials has not been reported.

In the present work, nanocomposites of PLA and MMT-clay were prepared by melt blending a PLLA-g-MMT nanohybrid, synthesized by ring-opening polymerization of L-lactide from the hydroxyl groups on the surface of Cloisite 30B, with a PLA matrix. Subsequently, a detailed investigation into the effect of PLLA-g-MMT addition on the morphology and crystallization of the PLA matrix was performed.

Experimental

Materials and methods

Poly(lactide (PLA) was supplied by NatureWorks under the trade name PLA 4032D with a D-lactide content of 2%. L-Lactide was supplied by Purac, which was recrystallized from dried toluene and stored in a glove box. 1,8-Diazabicyclo[5.4.0]undec-7-ene (DBU) and Amberlyst® 15 ion-exchange resin, in hydrogen form, were provided by Fluka. DBU was dried over BaO, distilled and stored in a glove box; Amberlyst® 15 was dried overnight at 60 °C. The clay used was Cloisite® 30B (Cl30B), which is an organically modified montmorillonite with 23.4% methyl bis(2-hydroxyethyl) tallowalkyl ammonium cations and was supplied by Southern Clay Products (USA). To synthesize Cloisite 30B-g-PLLA nanohybrids, PLLA was grafted on the clay surface by ring-opening polymerization (ROP) of L-lactide in the presence of 1,8-diazabicyclo[5.4.0]undec-7-ene (DBU) as a metal-free catalyst. In a glove box, y mmol of L-lactide was solubilized in $y/2$ mL of dry CHCl_3 and kept under a nitrogen atmosphere, and then the designed amount of Cl30B (10 wt%) was added. Then, 0.25 wt% DBU was equimolarly added upon the hydroxyl content present in the clay at room temperature. After 60 min, Amberlyst® 15 ion-exchange resin was added to quench the LA polymerization. The nanohybrid was recovered after precipitation in 8 volumes of *n*-heptane, filtered and dried overnight at 55 °C.²⁰ The amount of Cl30B in the nanohybrid was 10%. Gel permeation chromatography (GPC) was performed in CHCl_3 at 35 °C using a Polymer Laboratories liquid chromatograph equipped with a PL-DG802 degasser, an LC 1120 isocratic HPLC pump (flow

rate = 1 ml min⁻¹), a refractive index detector (ERMA 7517), an automatic injector (Polymer Laboratories GPC-RI/UV) and three columns: a PL gel 10 μm guard column and two PL gel mixed-B 10 μm columns. PS standards were used for calibration. The number average molecular weights measured by GPC were 9000 g mol⁻¹ for the PLLA grafted chains and 123 kg mol⁻¹ for commercial PLA 4032D.

Nanocomposite preparation

PLA and PLA-based nanocomposites were prepared by melt blending. PLA was blended with the PLLA-based nanohybrids using a DSM twin-screw microcompounder. The major processing parameters were mixing temperature, screw speed and residence time; they were set at 190 °C, 60 rpm and 10 min, respectively. All the PLA-based nanocomposites were made with an inorganic content of 5%. Samples produced for this study are specified in Table 1.

For the sake of comparison, commercial high molecular weight PLA 4032D (PLA) and low molecular weight PLLA (9000 g mol⁻¹) were blended in a ratio of 55/45 wt/wt. The low molecular weight PLLA was obtained by specific Soxhlet extraction from dichloromethane of low molecular weight PLLA chains coming from PLLA-g-MMT nanocomposites. PLA and PLLA were dissolved in a common solvent, chloroform, and the blend was cast on cover glasses. When chloroform was evaporated, the PLA/PLLA blend was dried under vacuum until constant mass was obtained.

Morphological analysis

The morphology of the nanocomposites was analysed by X-ray scattering (WAXS and SAXS) and transmission electron microscopy (TEM). TEM samples were 30–40 nm ultrathin sections obtained by employing an ultramicrotome. The samples were observed in a Tecnai G2 20 Twin microscope at an accelerating voltage of 200 kV.

SAXS experiments were performed using Rigaku 3-pinhole PSAXS-L equipment operating at 45 kV and 0.88 mA. The MicroMax-002+ X-ray generator system is composed of a microfocussed sealed tube source module and an integrated X-ray generator unit, which produces CuKα transition photons of wavelength $\lambda = 1.54 \text{ \AA}$. The scattered X-rays are detected on a two-dimensional multiwire X-ray detector (Gabriel design, 2D-200X). This gas-filled proportional-type detector offers a 200 mm diameter active area with *ca.* 200 μm resolution. The azimuthally averaged scattered intensities were obtained as a function of wave vector q , $q = 4\pi\lambda^{-1} \sin \theta$, where θ is half the scattering angle. Reciprocal space calibra-

tion was carried out using silver behenate as a standard. The flight path and the sample chamber in this equipment are under vacuum. SAXS was also conducted to probe the lamellar structure within the spherulites by determining their long periods.

WAXS measurements were performed at room temperature using a Bruker D8 Advance diffractometer working in parallel beam geometry. By using a Göbel mirror, the originally divergent incident X-ray beam from a line focus X-ray tube (Cu, operating at 40 kV and 40 mA) was transformed into an intense and parallel beam that is free of Kβ radiation. The parallel beam optics required in the secondary beam path was achieved with an equatorial axial Soller slit of 0.2°. LYNXEYE, the linear detector used, presents an active area of 14.4 mm × 16 mm. Measurements were carried out in reflection (θ - 2θ configuration) varying 2θ from 4 to 30° with a step of 0.05° and the measuring time employed was 10 s per point.

The spherulitic morphologies and the nucleation of the samples were observed by polarized light optical microscopy (PLOM) using a Leitz Aristomet polarized microscope equipped with a polarizer and a sensitive red tint plate (this was employed to determine the sign of the spherulites). A Mettler FP82Ht hot stage was used to control the temperature. The samples were pressed on a glass slide and covered with a glass coverslip. They were heated to 180 °C for 3 min and then they were quickly cooled to the selected crystallization temperature. Micrographs were taken with a Leica DC420 digital camera.

Thermal analysis

Thermogravimetric (TGA) analyses were performed from room temperature to 800 °C in a TG-Q500 TA Instruments thermal analyser at a heating ramp of 10 °C min⁻¹, under nitrogen flow. The unburnt residue left at 700 °C was used to calculate the nanoclay content in the PLA matrix.

The thermal properties of the polymer samples were investigated by differential scanning calorimetry (DSC), using a PerkinElmer Pyris 1 calorimeter equipped with a refrigerated cooling system (Intracooler 2P), under nitrogen atmosphere flow and calibrated with indium. The non-isothermal crystallization of the samples was investigated by first heating them to 180 °C at a heating rate of 10 °C min⁻¹, then recording the cooling scans from 180 down to 0 °C at the same rate, and finally performing a second heating scan from 0 to 180 °C also at the same rate of 10 °C min⁻¹.

The commercial PLA sample employed in this work is a slow-crystallizing polymer because of its 2% D-lactide

Table 1 Codes and summary of different blend compositions of PLA and PLA with an inorganic content of 5%

Sample	PLA	Cl30B	Cl30B-g-PLLA	Inorg content ^a [%]	T_{peak} [°C]
PLA 4032D	100				394
PLA/Cl30B	95	5		5	396
PLA/Cl30B-g-PLLA	50		50	5.5	387

^a Obtained by TGA.

stereoisomer content randomly distributed along the chains and its high molecular weight.²¹ Therefore, it was impossible to perform overall isothermal crystallization experiments in the DSC by directly quenching the sample from the melt to the crystallization temperature. However, if the sample is first cooled to the glassy state, nucleation can be enhanced^{22,23} and then the polymer is able to crystallize upon heating from the glassy state. Therefore, for isothermal crystallization experiments from the glassy state (see the thermal protocol in Fig. 1), samples were first heated to 180 °C for 3 min, in order to erase thermal history. Then, they were cooled at 60 °C min⁻¹ to 0 °C (a temperature below the T_g of PLA) to induce nucleation. Finally, the samples were heated at a rate of 60 °C min⁻¹ to the different crystallization temperatures (T_c) at which the isothermal crystallization process was monitored by DSC.

The procedure to determine the isothermal crystallization experiments and their modelling by the Avrami equation closely followed the method suggested by Lorenzo *et al.*²⁴ The free origin plugin developed by Lorenzo *et al.* was employed to perform the fittings to the Avrami equation.

Results and discussion

Thermogravimetric analysis (TGA)

The thermal stability of the nanocomposites was investigated by TGA under nitrogen flow at a heating rate of 20 °C min⁻¹. To characterize the thermal stability, some useful characteristic parameters can be considered such as the degradation temperature at the maximum rate of mass conversion (T_{peak}) and the fraction, which is not volatile at 700 °C, expressed as inorganic content. The results for neat PLA and for all the PLA-based nanocomposites are shown in Fig. 2 and the data are summarized in Table 1.

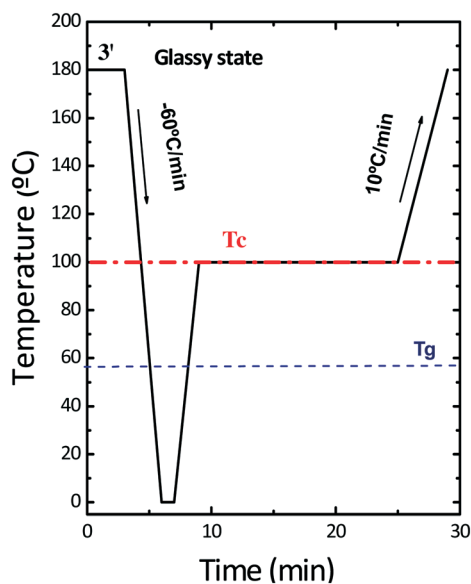


Fig. 1 Thermal program used for isothermal scans.

For all samples, single-step thermal degradation is observed in Fig. 2 corresponding to PLA degradation.²⁵ The results show that the neat PLA 4032D has a degradation temperature T_{peak} of 394 °C, while the nanocomposites based on PLA and Cloisite® 30B exhibit T_{peak} exceeding this value, suggesting higher thermal resistance, probably due to the effect of the inorganic filler. The nanoclay acts as a barrier, decreasing the diffusion of oxygen and volatile degradation products, which enhances the overall thermal stability of the system.²⁶ On the other hand, the nanohybrid-based composites presented a T_{peak} of 382 °C, *i.e.*, at a lower value in comparison to the value recorded for neat PLA. This result can be explained by the lower molecular weight of the PLLA chains grafted on the clay surface.

The nanocomposites were prepared by melt blending with an inorganic content of 5% and this content is confirmed by TGA. The values for the residue, detected at 700 °C, show that the desired inorganic content was achieved for all the nanocomposites prepared.

Crystal morphology and nanoclay dispersion

The addition of Cloisite® 30B or the nanohybrid to the PLA matrix was carried out by melt blending. The improvements in the material properties depend on the dispersion quality of the nanoclays.^{5,27} Clay dispersion was examined by X-ray scattering and TEM.

In Fig. 3, the WAXS and SAXS (inserts) diffractograms of neat PLA and the PLA/Cl30B and PLA/Cl30B-g-PLLA nanocomposites crystallized isothermally at a T_c of 120 °C for 24 h are shown. The most intense reflections for all samples appear at $2\theta = 14.8, 16.6$ and 19.0° , and they can be indexed to (010), (110), (200), and (203) planes of the α -form of PLLA, crystallized in a pseudo-orthorhombic unit cell of dimensions $a = 1.07, b = 0.595$ and $c = 2.78$ nm, which contains two 10₃ helices.^{20,28}

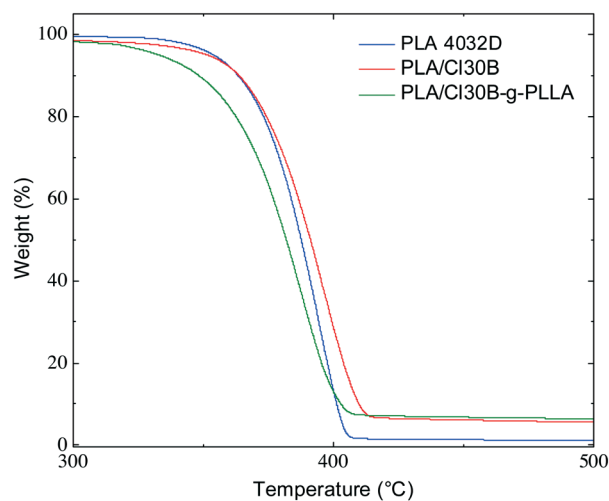


Fig. 2 TGA curves from thermogravimetric analysis under nitrogen flow, at 10 °C min⁻¹ for PLA 4032D and the nanocomposites.

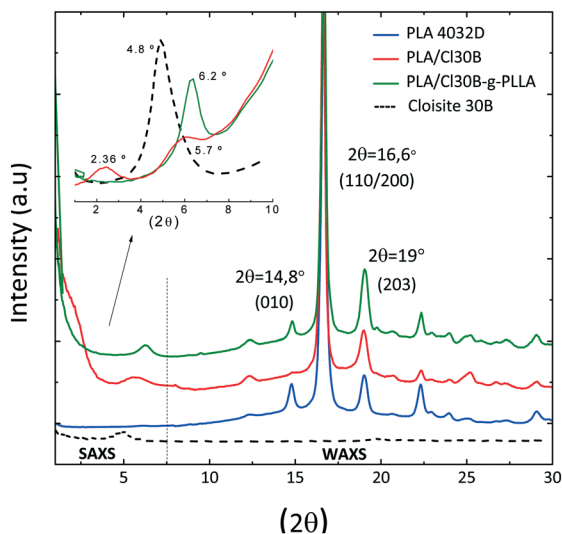


Fig. 3 SAXS (low angle) and WAXS (high angle) diffraction patterns of samples crystallized at 120 °C for 24 h.

The degree of clay dispersion in the nanocomposites can be deduced by the low angle reflections. As expected, between 2 and 8°, no peak is observed in the diffractogram of neat PLA as it contains no clay. On the other hand, neat Cloisite® 30B exhibits a sharp peak at around 4.8°, corresponding to an interlayer spacing of 1.8 nm.^{20,26}

In the case of the PLA/Cl30B nanocomposite, the peak corresponding to the nanoclay is shifted to a lower angle, with a 2θ value of 2.36°, in SAXS, corresponding to an increase of d -spacing to 3.6 nm. This increase results from the intercalation of polymer chains inside the clay layers. The presence of peaks at $2\theta = 5.7^\circ$ can be assigned to the presence of nanoclay aggregates (also observed by TEM, see Fig. 4a).²⁹

As far as the PLA/Cl30B-g-PLLA nanocomposite is concerned, no diffraction peak can be observed within the low angle region, studied by SAXS, indicating the complete exfoliation of nanoclays within the PLA matrix. However, a peak at 6.2° is present in the grafted nanocomposite, assigned to regularly packed silicate tactoids with collapsed d -spacings. This d -spacing collapse or tightening of the silicate stacks is due to a change in disposition of the substituents of the quaternary ammonium ions into a more compact arrangement observed when Cl30B is molten at temperatures around 200 °C.³⁰

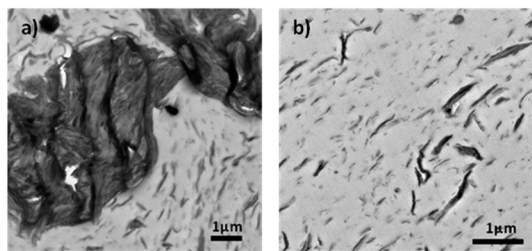


Fig. 4 TEM images of the nanocomposites (a) PLA/Cl30B and (b) PLA/Cl30B-g-PLLA with 5 wt% Cl30B.

Representative TEM micrographs are shown in Fig. 4. In both cases presented in the figure, exfoliated/intercalated structures can be observed, but more aggregates are observed in the sample that contains neat nanoclay (Fig. 4a). A better dispersion is clearly observed for the PLA/Cl30B-g-PLLA nanocomposite (Fig. 4b). The micrographs are consistent with the X-ray diffraction results presented above.

In order to show the effect of nanoclay on the crystal microstructure, the SAXS diffraction profiles of isothermally crystallized (at 120 °C for 24 h) PLA, PLA/Cl30B and PLA/Cl30B-g-PLLA are shown in Fig. 5. The Lorentz-corrected intensity (*i.e.*, $I \times q^2$) is plotted as a function of the scattering vector q . A pronounced peak can be observed in neat PLA corresponding to the X-ray scattering of the lamellar stacks. The peak intensity is substantially reduced in the samples containing nanoclay, as they interfere with the scattering from the lamellar stacks.

The maximum peak q_{\max} can be assigned to the long period of the PLA lamellar stack. The q_{\max} values were 0.031, 0.032 and 0.032 \AA^{-1} for neat PLA, PLA/Cl30B and PLA/Cl30B-g-PLLA nanocomposites, respectively. The d^* values were calculated from the q_{\max} values taken from the Lorentz-corrected plot using the following expression (eqn (1)):

$$d^* = 2\pi/q_{\max} \quad (1)$$

The estimated long period d^* values were 20.2, 19.6 and 19.8 nm for PLA, PLA/Cl30B and PLA/Cl30B-g-PLLA, respectively. Values of the same order of magnitude were obtained by Huang *et al.*³¹ for PLA crystallized at different temperatures. Furthermore, it is interesting to note that the d^* -spacing did not depend on the presence of clay or nanohybrids in the PLA matrix, indicating that the controlling factor for the

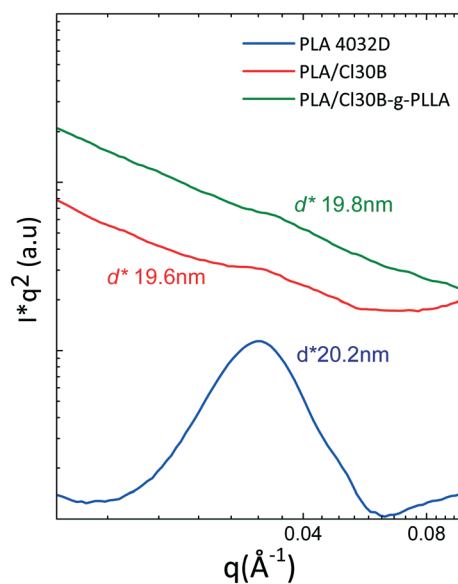


Fig. 5 Lorentz-corrected SAXS profiles, with intensity as a function of scattering vector, of selected samples.

ultimate lamellar thickness obtained after 24 h of crystallization was the supercooling applied.

The calculation of the lamellar thickness, l , was performed employing the following approximation:

$$l = d^* \cdot V_c \quad (2)$$

where V_c is the crystalline volume fraction that can be calculated from the following equation:

$$V_c = \frac{W_c}{W_c + \frac{\rho_c(1-W_c)}{\rho_a}} \quad (3)$$

where ρ_c and ρ_a are the fully crystalline and fully amorphous polymer densities, respectively. In this case, we have employed the following values that correspond to polylactide: $\rho_c = 1.36 \text{ g cm}^{-3}$ and $\rho_a = 1.25 \text{ g cm}^{-3}$.^{32,33} W_c is the crystalline mass fraction that can be calculated as:

$$W_c = \frac{\Delta H_m}{\Delta H_{100\%}} \quad (4)$$

taking ΔH_m as the enthalpy value for the samples after isothermal crystallization at 120 °C for 24 h followed by cooling to room temperature (44.6, 41.0 and 44.8 J g⁻¹ for neat PLA, PLA/Cl30B and PLA/Cl30B-g-PLLA, respectively) and $\Delta H_{100\%}$ as the enthalpy of fusion for a 100% crystalline polymer sample (93.1 J g⁻¹).

The calculated lamellar thickness values for neat PLA, PLA/Cl30B and PLA/Cl30B-g-PLLA are 9.3, 8.3 and 9.1 nm, respectively. Therefore, no significant variation was obtained for the three different samples as the lamellar thickness depends on the supercooling applied. Cho *et al.* reported lamellar thickness values of 12.3 and 10.7 nm for samples PLLA and 3% *meso*-lactide, respectively, crystallized at 123 °C.³⁴

Non-isothermal DSC experiments

The study of the crystallization was carried out on neat PLA, PLA/Cl30B, PLA/Cl30B-g-PLLA and also on a PLA/PLLA blend for the sake of comparison. The heating scans after cooling the samples from the melt (at 10 °C min⁻¹) are reported in Fig. 6 and the main results are summarized in Table 2.

Neither neat PLA nor PLA-based nanocomposites are able to crystallize during cooling (see Fig. 1S in the ESI†) at the scanning rate employed (10 °C min⁻¹). It is known that the presence of a low percentage of the *D*-isomer (2% of *D*-isomer for PLA 4032D) slows down the crystallization process of poly(lactic acid).²¹ Nevertheless, the PLA/PLLA blend presents a small crystallization peak during cooling, suggesting a higher crystallization rate at the scanning rate employed.

On the other hand, Fig. 6 shows important differences between the samples when they are heated after previous cooling from the melt to the glassy state. Neat PLA exhibits a clear T_g and undergoes a broad and barely noticeable cold

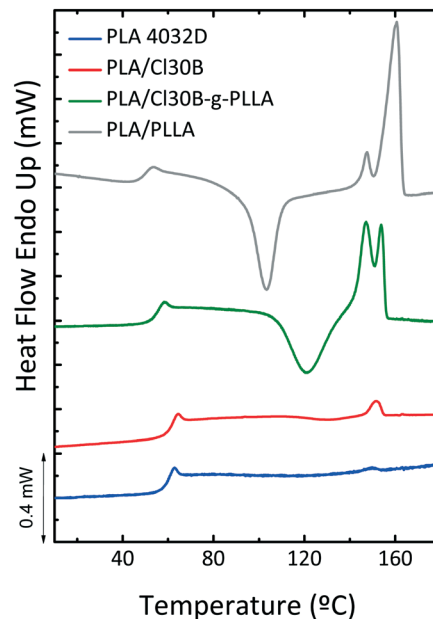


Fig. 6 DSC heating scans for the indicated samples after cooling them previously from the melt at 10 °C min⁻¹.

crystallization (in the range of 100–140 °C) followed by the melting of the formed crystals in a small endotherm. The behaviour of the PLA/Cl30B nanocomposite is very similar to that of neat PLA, although the enthalpy of cold crystallization (and correspondingly the enthalpy of melting) is slightly higher, possibly indicating a slight increase in the non-isothermal crystallization rate upon heating caused by a small nucleating effect of the nanoclay.

The PLA/Cl30B-g-PLLA sample shows an enhanced capacity for crystallization during heating from the glassy state, as indicated by the large cold crystallization exotherm followed by melting. These results suggest that the presence of the nanohybrid increases the non-isothermal crystallization rate from the vitreous state. The double melting peak observed is commonly ascribed to the melting and recrystallization events that occur during the heating scan.³⁵ Additionally, the heating DSC scan of the PLA/PLLA sample is similar to that of the nanohybrid nanocomposites, even when no nanoclay is present in this blend sample.

Table 2 shows that within the error involved in the measurements, the enthalpies of cold crystallization and melting are the same for the three samples. This confirms the impossibility for the PLA employed to crystallize during the previous cooling at 10 °C min⁻¹.

Table 2 Relevant parameters obtained from the DSC heating scans shown in Fig. 6 for the PLA, PLA/Cl30B and PLA/Cl30B-g-PLLA samples

	T_g (°C)	T_c	ΔH_c	T_{cc} (°C)	ΔH_{cc}	T_m (°C)	ΔH_m
PLA 4032D	57			128	-0.3	150	0.5
PLA/Cl30B	58			127	-0.9	151	1.1
PLA/Cl30B-g-PLLA	53			121	-27.9	147/154	27.3
PLA/PLLA	48	91.4	-4.1	103	-29.8	147/160	35.2

Table 2 also shows that neat PLA exhibits a T_g of 57 °C. The addition of neat Cloisite 30B to PLA does not significantly affect the T_g value (there is an increase of 1 °C). However, when the nanohybrid or low M_n PLLA is added to PLA, the T_g decreases by 4 °C and 9 °C, respectively. This decrease in T_g is caused by the addition of low molecular weight PLLA chains present in both nanohybrids and blend samples. These short PLLA chains act as plasticizers for the high molecular weight PLA matrix ($M_n = 123 \text{ kg mol}^{-1}$) causing a T_g depression and an increase in the non-isothermal crystallization rate from the glassy state.³⁶

Spherulitic growth kinetics of PLA and nanocomposites from the melt

In the case of PLOM measurements, one can afford to wait until PLA spherulites grow directly from the melt, even if they take a long time to do so. Fig. 7 shows the spherulitic morphology of neat PLA and its nanocomposites and of the PLA/PLLA blend, crystallized from the melt at $T_c = 125$ °C. Negative PLA spherulitic superstructures with characteristic Maltese cross extinction patterns are observed for all samples.³⁷ In the micrograph of the nanocomposite PLA/Cl30B, clay aggregates can be observed both inside the spherulites and outside in the melt. On the other hand, the spherulites corresponding to the nanohybrid PLA/Cl30B-g-PLLA (Fig. 7c) exhibit clear Maltese cross extinction patterns without signs of the clay. This means that nanoclay aggregates are too small (approx. smaller than 1 μm) to be observed with an optical microscope as a better dispersion is obtained in the nanohybrid case (as indicated in the TEM micrograph in Fig. 4b). A similar spherulitic morphology is observed for the PLA/PLLA blend (Fig. 7d).

All PLA spherulites grew linearly with time without encountering any diffusion problems. From the slope of the straight line obtained by plotting the spherulitic radius (μm)

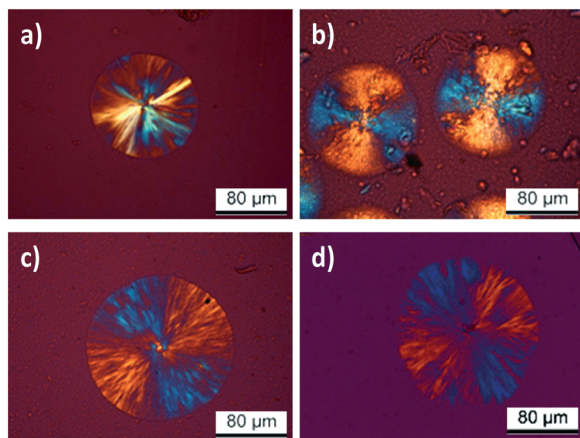


Fig. 7 Spherulitic morphology of the following melt crystallized materials observed by PLOM, at a crystallization temperature of 125 °C: (a) PLA 4032D, (b) PLA/Cl30B, (c) PLA/Cl30B-g-PLLA and (d) PLA/PLLA.

versus time (min), the spherulitic growth rate G ($\mu\text{m min}^{-1}$) was obtained.

The spherulitic growth rate from the melt is represented as a function of the isothermal crystallization temperature in Fig. 8. The expected bell-shaped curve is obtained for neat PLA, the nanocomposites and the blend, where the left hand side corresponds to the trend determined by diffusion control while the right hand side is determined by nucleation control. No discontinuity is observed in the curves of G versus T_c , as has been reported in the literature when PLA exhibits both α and α' phases (see ref. 38). In the present case, only the α phase was formed in the T_c range studied.

Fig. 8 shows that neat PLA with or without Cl30B has similar spherulitic growth rates in the temperature range examined. On the other hand, for PLA/Cl30B-g-PLLA, the G values obtained are significantly higher than those for neat PLA and PLA/Cl30B. At a crystallization temperature of 118 °C, for example, the PLA/PLLA spherulites in the samples that contain the Cl30B-g-PLLA nanohybrid grow three times faster than those of neat PLA. This remarkable result can be attributed to the plasticizing effect of the low molecular weight polylactic acid chains grafted to the nanoclay. It must be remembered that the PLA/Cl30B-g-PLLA sample contains approx. 45% low M_n PLLA chains, 5% clay and 50% high M_n PLA. The low M_n PLLA chains are miscible with the high M_n PLA chains leading to a lower T_g and a reduction in the energy barrier required for crystallization. For the neat PLA/PLLA blend, the G values are even higher than those for PLA/Cl30B-g-PLLA, thus confirming the plasticizing effect of the low M_n PLLA chains in the blend significantly increasing the spherulitic growth rate of PLA.

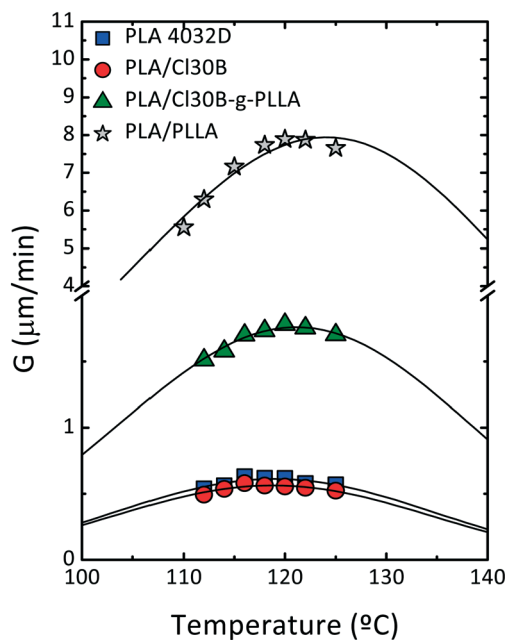


Fig. 8 Spherulitic growth rate as a function of crystallization temperature for the PLA and PLA nanocomposites. Continuous lines correspond to the fit of the Lauritzen-Hoffman theory.

Comparable increases in spherulitic growth rates are reported for plasticized PLA with polyethylene glycol (PEG).^{39,40} However, in PLA/PEG blends, the plasticizing effect is affected by aging, during which phase segregation has been reported. In this respect, the use of Cl30B-g-PLLA employed in this work represents an improvement since it does not phase segregate from PLLA. Additionally, Cl30B could provide barrier properties.

The solid lines in Fig. 8 are fits to the experimental data obtained with the Lauritzen and Hoffman theory (LH). According to this well-known nucleation and growth theory, the spherulitic growth rate $G(T)$ can be expressed as a function of supercooling according to:^{41,42}

$$G(T) = G_0 \exp\left(\frac{-U^*}{R(T_c - T_\infty)}\right) \exp\left(\frac{-K_g^G}{T_c \Delta T f}\right) \quad (5)$$

where G_0 is a pre-exponential growth rate constant, U^* is the activation energy for the transport of the chains to the growing front (a value of $1500 \text{ cal mol}^{-1}$ is usually employed), R is the gas constant, and T_c is the isothermal crystallization temperature. T_∞ is the temperature at which chain mobility ceases and it is usually taken as $T_g - 30 \text{ (K)}$. ΔT is the supercooling defined as $(T_m^0 - T_c)$, where T_m^0 is the equilibrium melting point; a value of $215 \text{ }^\circ\text{C}$ is employed here, and the values are taken from a previous paper.⁴³ The factor f is a temperature correction term equal to $2T_c/(T_c + T_m^0)$, and K_g is a secondary nucleation constant, which can be considered proportional to the energy barrier for secondary nucleation.

The results obtained from the Lauritzen–Hoffman fits are listed in Table S1.† The fitting shows good agreement with the experimental data throughout the entire crystallization temperature range.

The secondary nucleation constant values, K_g^G , are plotted in Fig. 9. It can be observed that the K_g^G values obtained for neat PLA are much higher than those for PLA/Cl30B, PLA/Cl30B-g-PLLA and PLA/PLLA, as depicted in Fig. 9. The results are expected on the basis of the crystallization ability of

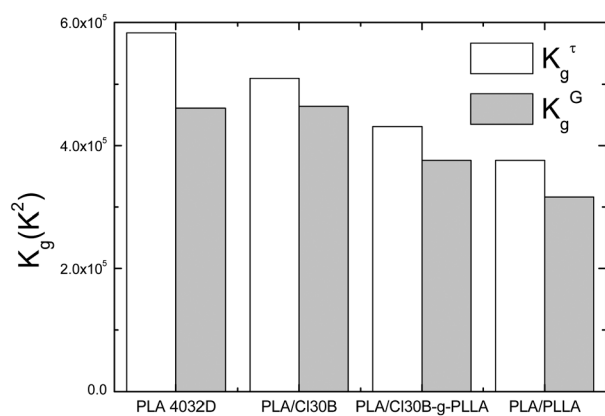


Fig. 9 The K_g^G and K_g^τ parameters derived from the LH fittings are plotted as a function of the samples.

each system. Since PLA/PLLA and PLA/Cl30B-g-PLLA exhibit faster spherulitic growth rates than neat PLA, a lower energy barrier for spherulitic growth is expected (and therefore a lower K_g^G value).

Overall crystallization rate from the glassy state

The inverse of the half-crystallization time, determined by means of DSC isothermal crystallization experiments, is an experimental measure of the overall crystallization rate that includes both nucleation and growth.

Fig. 10 shows the overall crystallization rate (expressed as $1/\tau_{50\%}$) as a function of temperature for neat PLA, the nanocomposites and the PLA/PLLA blend. The isothermal crystallization experiments were performed from the glassy state, as explained in the experimental section and in Fig. 1. Having neat PLA as a reference material, the crystallization rate increases slightly by blending the material with Cloisite® 30B nanoclay (see Fig. 10). As it was previously shown that the spherulitic growth is unaffected by the presence of clay (see Fig. 8), this small increase in overall crystallization rate can be merely due to the nucleation effect of nanoclay. In the case of the PLA/Cl30B-g-PLLA nanocomposite, the crystallization rate is approximately six times higher than that of neat PLA, while for the PLA/PLLA blend, the increase is twelve times higher. These remarkable increases in overall crystallization rate are caused by the plasticizing effect of the low molecular weight PLLA chains that are present in the samples. Jia *et al.* found similar effects for plasticized PLA blends. With the incorporation of PEG and PEPG as plasticizers, the crystallization rate of PLA increased. They

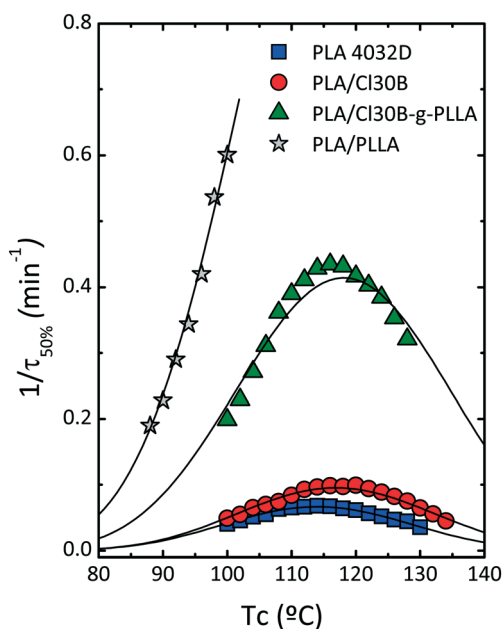


Fig. 10 Overall crystallization rate as a function of the crystallization temperature of PLA nanocomposites. Continuous lines correspond to the theoretical prediction of the Lauritzen–Hoffman theory.

reported decreases in $t_{1/2}$ from 5.44 min in neat PLA to 0.93 min in PLA with 20 wt% PEPG.⁴⁴ In the case of the nanohybrids, the advantage is the impossibility of leaching out of the “surface-grafted plasticizer” (*e.g.*, Cl30B-*g*-PLLA), so no phase separation can occur from the PLA matrix, in contrast with other blends, like for instance, PLA/PEG blends.

The Lauritzen and Hoffman theory can also be applied to DSC data if $G(T)$ in eqn (5) is replaced by the inverse of the experimental half-crystallization time.⁴⁵ Therefore, the continuous lines shown in Fig. 10 correspond to the Lauritzen–Hoffman fits for the overall crystallization rate. The parameters derived from the application of the theory are summarized in Table S2† and the K_g^x values are plotted in Fig. 9. In this case, K_g^x is proportional to the total energy barrier for the overall crystallization (*i.e.*, for both nucleation and growth).

The reduction in the overall crystallization rate produces an increase in the values of K_g^x , so the K_g^x values for neat PLA are much higher than those for PLA/Cl30B, PLA/Cl30B-*g*-PLLA and PLA/PLLA as observed in Fig. 9. Moreover, in all the samples, K_g^G values are smaller than K_g^x values, as shown in Fig. 9. This result is also expected since K_g^G values only consider the growth contribution to the free energy of crystallization, while in K_g^x , both nucleation and growth contributions are included.⁴¹

The overall crystallization rate can also be modelled by the Avrami equation:⁴⁶

$$1 - V_c(t - t_0) = \exp(-k(t - t_0)^n) \quad (6)$$

where t is the experimental time, t_0 is the induction time, V_c is the relative volumetric transformed fraction, n is the Avrami index and k is the overall crystallization rate constant. The fits to the Avrami equation were obtained using the Origin plug-in developed by Lorenzo *et al.*²⁴

The results obtained are presented in Table S3† and Fig. 11 shows one example of the good agreement between the Avrami model and the experimental data. Fig. 11a shows a comparison between the experimental and the predicted DSC isothermal scans. Fig. 11c shows that the Avrami equation can perfectly describe the overall crystallization kinetics of PLA in the primary crystallization range (with a correlation coefficient of 1.000), before the spherulites impinge on one another, in a conversion range up to 25%. The fit is also quite good for the particular case of PLA up to much higher conversion, as shown in Fig. 11a and b.

For the isothermal crystallization of PLA or the PLA phase of all the nanocomposites, the Avrami index value (n) oscillated between 2.5 and 4 (see Fig. 12a). By PLOM, spherulites were observed for all the samples (Fig. 7), so Avrami index values of 2.5–4 are expected, since $n = 3$ corresponds to instantaneously nucleated spherulites and $n = 4$ to sporadically nucleated spherulites.^{24,47}

Another result that could be expected is an increase in Avrami index with crystallization temperature, as the nucle-

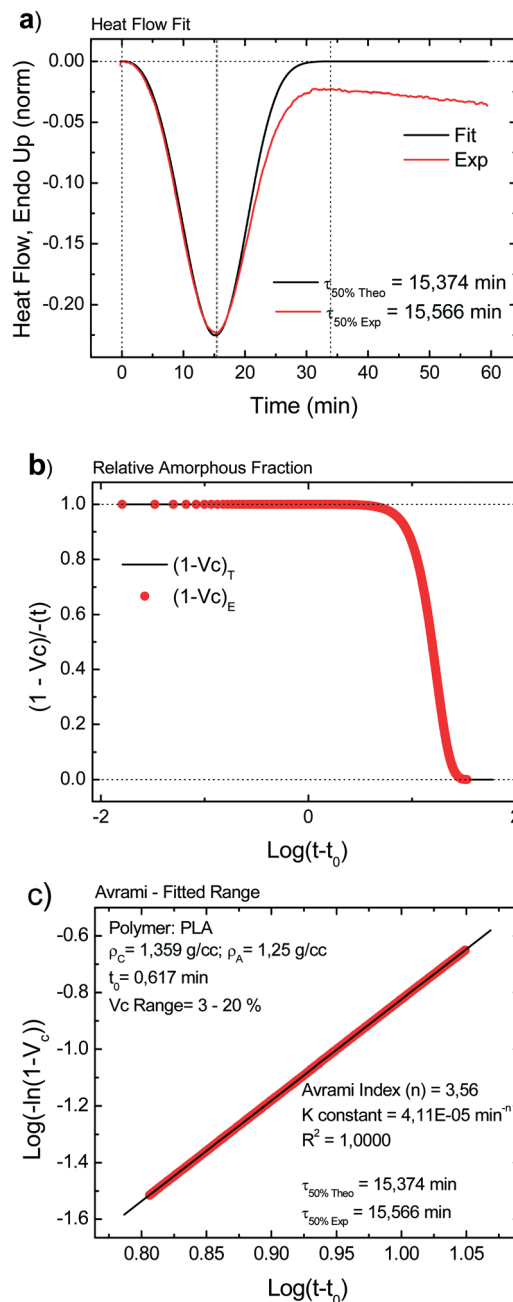


Fig. 11 (a–c) The fits to the Avrami equation using the Origin plug-in developed by Lorenzo *et al.*²⁴ and the experimental data for the PLA sample.

ation becomes more sporadic as supercooling decreases. This is indeed observed in Fig. 12a, except for the samples PLA/Cl30B-*g*-PLLA and PLA/PLLA blend where n appears constant with crystallization temperatures. For these systems, the effect of the low molecular weight PLLA chains may compensate for the nucleation trend.

The isothermal rate constant k has units that depend on n (*i.e.* min^{-n}). Therefore, it is difficult to compare its values as n changes with T_c and from sample to sample. One way to overcome this difficulty is to elevate k to $1/n$, so that all

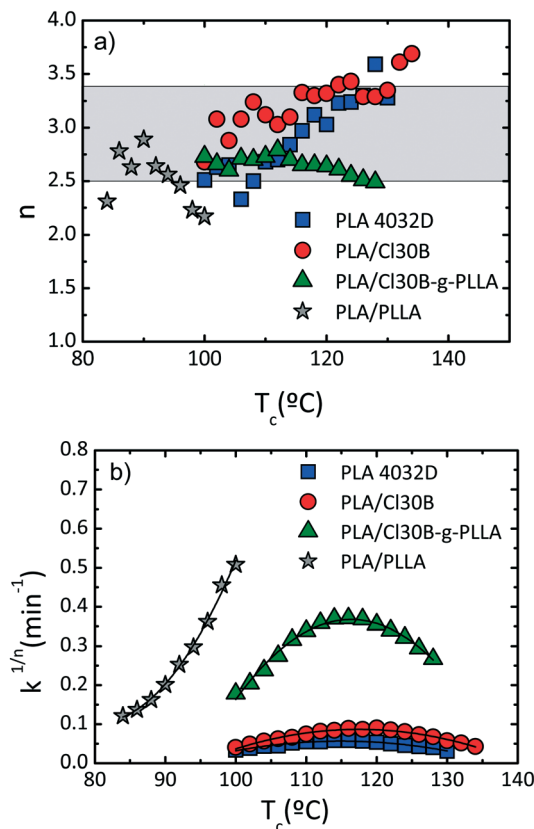


Fig. 12 (a) Avrami index (n) and (b) isothermal crystallization rate constant as a function of crystallization temperature. The solid lines represent arbitrary fits to guide the eye.

values of k are expressed in reciprocal time units (in this case, min⁻¹). These functions, $k^{1/n}$, are plotted in Fig. 12b as a function of T_c . The remarkable similarity with Fig. 10 is a consequence of the excellent fit of the Avrami equation to the overall crystallization rate data.

According to the above results, both PLA/PLLA and PLA/Cl30B-g-PLLA samples have higher crystallization rates than neat PLA and PLA/Cl30B, mainly because of the presence of low molecular weight PLLA chains.

Even so, the differences in crystallization rate between the PLA/PLLA blend and the PLA/Cl30B-g-PLLA nanocomposite are quite substantial. The difference between both samples is due to the presence of the Cl30B-g-PLLA component. In such a hybrid material, low molecular weight PLLA chains are covalently linked to the ammonium cations covering the surface of well-dispersed nanoclay platelets. Such chain tethering on the surface of mostly exfoliated nanoclays restricts the mobility of the PLLA chains in comparison with free PLLA molecules. Free low M_n PLLA chains can act as better plasticizing agents for high M_n PLA in comparison with chains tethered at the nanoclay surfaces. Clear evidence of the difference in overall chain mobility is given in Table 2, as the T_g value decreases from a value of 56 °C for neat PLA to 53 °C for the PLA/Cl30B-g-PLLA nanocomposite and to a minimum of 48 °C for the PLA/PLLA blend.

Conclusions

The plasticizing effect of low molecular weight PLLA chains (9 kg mol⁻¹) can substantially accelerate both the spherulitic growth and the overall crystallization rate of commercial PLA 4032D. Their accelerating effect on the nucleation and crystallization of PLA is reduced but still substantial when these low M_n PLLA chains are grafted to nanoclay platelets. The advantage of using low M_n PLLA chains as internal plasticizers for PLA is their non-leachable character.

Acknowledgements

The POLYMAT-UPV/EHU team would like to acknowledge funding from the following projects: UPV/EHU (UFI 11/56); GIC IT-586-13 (Basque Government); UPV/EHU Infrastructure: INF 14/38; Mineco/FEDER: SINF 130I001726XV1/Ref: UNPV13-4E-1726; Mineco MAT2014-53437-C2-P. Nerea Zaldúa acknowledges the fellowship from the University of Basque Country UPV/EHU. A. A. and A. I. acknowledge financial support from the Spanish Ministry 'Ministerio de Economía y Competitividad', code: MAT2015-63704-P (MINECO/FEDER, UE) and the Basque Government, code: IT-654-13.

References

- 1 P. Bordes, E. Pollet and L. Avérous, *Prog. Polym. Sci.*, 2009, **34**, 125–155.
- 2 K. Hamad, M. Kaseem, H. W. Yang, F. Deri and Y. G. Ko, *eXPRESS Polym. Lett.*, 2015, **9**, 435–455.
- 3 A. J. R. Lasprilla, G. A. R. Martinez, B. H. Lunelli, A. L. Jardini and R. M. Filho, *Biotechnol. Adv.*, 2012, **30**, 321–328.
- 4 E. Ruiz-Hitzky and F. M. Fernandes, *Prog. Polym. Sci.*, 2013, **38**, 1391.
- 5 J.-M. Raquez, Y. Habibi, M. Murariu and P. Dubois, *Prog. Polym. Sci.*, 2013, **38**, 1504–1542.
- 6 S. Sinha Ray, P. Maiti, M. Okamoto, K. Yamada and K. Ueda, *Macromolecules*, 2002, **35**, 3104–3110.
- 7 S. Sinha Ray and M. Okamoto, *Prog. Polym. Sci.*, 2003, **28**, 1539–1641.
- 8 S. J. Ahmadi, Y. D. Huang and W. Li, *J. Harbin Inst. Technol.*, 2004, **11**, 138–145.
- 9 S. Pavlidou and C. D. Papaspyrides, *Prog. Polym. Sci.*, 2008, **33**, 1119–1198.
- 10 S. K. Kumar, N. Jouault, B. Benicewicz and T. Neely, *Macromolecules*, 2013, **46**, 3199–3214.
- 11 B. Lepoittevin, N. Pantoustier, M. Devalckenaere, M. Alexandre, D. Kubies, C. Calberg, R. Jérôme and P. Dubois, *Macromolecules*, 2002, **35**, 8385–8390.
- 12 M. A. Paul, M. Alexandre, P. Degée, C. Calberg, R. Jérôme and P. Dubois, *Macromol. Rapid Commun.*, 2003, **24**, 561–566.
- 13 A. Kiersnowski and J. Pięłowski, *Eur. Polym. J.*, 2004, **40**, 1199–1207.
- 14 L. Liao, C. Zhang and S. Gong, *Macromol. Rapid Commun.*, 2007, **28**, 1148–1154.

- 15 M. A. Paul, C. Delcourt, M. Alexandre, P. Degee, F. Monteverde, A. Rulmont and P. Dubois, *Macromol. Chem. Phys.*, 2005, **206**, 484–498.
- 16 L. Urbanczyk, F. Ngoundjo, M. Alexandre, C. Jérôme, C. Detrembleur and C. Calberg, *Eur. Polym. J.*, 2009, **45**, 643–648.
- 17 J. T. Yoon, G. Jeong, S. C. Lee and B. G. Min, *Polym. Adv. Technol.*, 2009, **20**, 631–638.
- 18 J. T. Yoon, S. C. Lee and Y. G. Jeong, *Compos. Sci. Technol.*, 2010, **70**, 776–782.
- 19 A. L. Goffin, J. M. Raquez, E. Duquesne, G. Siqueira, Y. Habibi, A. Dufresne and P. Dubois, *Biomacromolecules*, 2011, **12**, 2456–2465.
- 20 G. Lo Re, S. Benali, Y. Habibi, J.-M. Raquez and P. Dubois, *Eur. Polym. J.*, 2014, **54**, 138–150.
- 21 A. J. Müller, M. Ávila, G. Saenz and J. Salazar, Crystallization of PLA-based Materials, in *Poly(lactic acid) Science and Technology: Processing, Properties, Additives and applications*, ed. A. Jimenes, M. Peltzer and R. Ruseckaite, 2015, ch. 3, pp. 66–98, DOI: 10.1039/9781782624806-00066, RSC Polymer Chemistry Series.
- 22 E. Quero, A. J. Müller, F. Signori, M.-B. Coltelli and S. Bronco, *Macromol. Chem. Phys.*, 2012, **213**, 36–48.
- 23 R. Liao, B. Yang, W. Yu and C. Zhou, *J. Appl. Polym. Sci.*, 2007, **104**, 310–317.
- 24 A. T. Lorenzo, M. L. Arnal, J. Albuerné and A. J. Müller, *Polym. Test.*, 2007, **26**, 222–231.
- 25 M. Iturrondobeitia, A. Okariz, T. Guraya, A. M. Zaldúa and J. Ibarretxe, *J. Appl. Polym. Sci.*, 2014, **131**, 9120–9127.
- 26 L. Zaidi, S. Bruzard, A. Bourmaud, P. Médéric, M. Kaci and Y. Grohens, *J. Appl. Polym. Sci.*, 2010, **116**, 1357–1365.
- 27 A. Vermogen, K. Masenelli-Varlot, R. Séguéla, J. Duchet-Rumeau, S. Boucard and P. Prele, *Macromolecules*, 2005, **38**, 9661–9669.
- 28 J. K. Palacios, A. Mugica, M. Zubitur, A. Iturrospe, A. Arbe, G. Liu, D. Wang, J. Zhao, N. Hadjichristidis and A. J. Müller, *RSC Adv.*, 2016, **6**, 4739–4750.
- 29 N. Tenn, N. Follain, J. Soulestin, R. Crétois, S. Bourbigot and S. Marais, *J. Phys. Chem. C*, 2013, **117**, 12117–12135.
- 30 S. Filippi, M. Paci, G. Polacco, N. T. Dintcheva and P. Magagnini, *Polym. Degrad. Stab.*, 2011, **96**, 823–832.
- 31 J. Huang, M. S. Lisowski, J. Runt, E. S. Hall, R. T. Kean, N. Buehler and J. S. Lin, *Macromolecules*, 1998, **31**, 2593–2599.
- 32 K. Madhavan Nampoothiri, N. R. Nair and R. P. John, *Bioresour. Technol.*, 2010, **101**, 8493–8501.
- 33 A. G. M. L. Lu, Poly(lactic acid), in *Polymer Data Handbook*, 1999.
- 34 J. Cho, S. Baratian, J. Kim, F. Yeh, B. S. Hsiao and J. Runt, *Polymer*, 2003, **44**, 711–717.
- 35 Z. Wei, P. Song, C. Zhou, G. Chen, Y. Chang, J. Li, W. Zhang and J. Liang, *Polymer*, 2013, **54**, 3377–3384.
- 36 A. Ruellan, V. Ducruet and S. Domenek, Plasticization of Poly(lactide), in *Poly(lactic acid) Science and Technology: Processing, Properties, Additives and applications*, ed. A. Jimenes, M. Peltzer and R. Ruseckaite, 2015, ch. 5, pp. 124–170, DOI: 10.1039/9781782624806-00066, RSC Polymer Chemistry Series.
- 37 G. Lugito and E. M. Woo, *Colloid Polym. Sci.*, 2013, **291**, 817–826.
- 38 R. Androsch, M. L. Di Lorenzo and C. Schick, *Eur. Polym. J.*, 2016, **75**, 474–485.
- 39 E. Piorkowska, Z. Kulinski, A. Galeski and R. Masirek, *Polymer*, 2006, **47**, 7178–7188.
- 40 H. Li and M. A. Huneault, *Polymer*, 2007, **48**, 6855–6866.
- 41 J. I. Lauritzen and J. D. Hoffman, *J. Res. Natl. Bur. Stand., Sect. A*, 1960, **64**, 73–102.
- 42 J. D. Hoffman and J. I. Lauritzen, *J. Res. Natl. Bur. Stand., Sect. A*, 1961, **65**, 297–336.
- 43 H. Abe, M. Harigaya, Y. Kikkawa, T. Tsuge and Y. Doi, *Biomacromolecules*, 2005, **6**, 457–467.
- 44 Z. Jia, J. Tan, C. Han, Y. Yang and L. Dong, *J. Appl. Polym. Sci.*, 2009, **114**, 1105–1117.
- 45 A. T. Lorenzo and A. J. Müller, *J. Polym. Sci., Part B: Polym. Phys.*, 2008, **46**, 1478–1487.
- 46 A. Melvin, *J. Chem. Phys.*, 1941, **9**, 177.
- 47 J. M. Schultz, *Polymer Crystallization: The Development of Crystalline Order in Thermoplastic Polymers*, Oxford U. Press, Oxford, 2001.